Supplementary Materials

Engineering Si-bridge mediated g-C_3N_4/$NdFeO_3$ Z-scheme heterojunction for multifunctional catalytic applications: CO_2 conversion, organic pollutant degradation and H_2 production

Iltaf Khan[1,#], Saeed Zaman[2,#], Ali Bahadur[3], Anuj Kumar[4], Safura Bibi[5], Muhammad Hammad Zaman[6], Laiba Mujahid[7], Ghulam Yasin[8], Aftab Khan[9], Shoaib Khan[10]

[1]School of Chemical Science and Engineering, Tongji University, Shanghai 200092, China.
[2]School of Materials Science and Engineering, Harbin Institute of Technology (Shenzhen), Shenzhen 518055, Guangdong, China.
[3]Department of Chemistry, College of Science, Mathematics, and Technology, Wenzhou-Kean University, Wenzhou 325060, Zhejiang, China.
[4]Nano-Technology Research Laboratory, Department of Chemistry, GLA University, Mathura, Uttar Pradesh 281406, India.
[5]Department of Botany, University of Agriculture Faisalabad, Faisalabad 38040, Pakistan.
[6]School of Chemical Engineering and Technology, Tianjin University, Tianjin 300350, China.
[7]School of Environmental & Chemical Engineering, Jiangsu University of Science and Technology, Zhenjiang 212100, Jiangsu, China.
[8]School of Environment and Civil Engineering, Dongguan University of Technology, Dongguan 523808, Guangdong, China.
[9]State Key Laboratory of Chemical Resource Engineering, Beijing Advanced Innovation Center for Soft Matter Science and Engineering, College of Chemistry, Beijing University of Chemical Technology, Beijing 100029, China.
[10]Jiangsu Key Laboratory of Sericultural and Animal Biotechnology, School of Biotechnology, Jiangsu University of Science and Technology, Zhenjiang 212100, Jiangsu, China.
[#]Authors contributed equally.

Correspondence to: Dr. Iltaf Khan, School of Chemical Science and Engineering, Tongji University, Shanghai 200092, China. E-mail: doctoriltafkhan@tongji.edu.cn; Dr. Ali

Bahadur, Department of Chemistry, College of Science, Mathematics, and Technology, Wenzhou-Kean University, Wenzhou 325060, Zhejiang, China. E-mail: Abahadur@wku.edu.cn

1. Experimental Section

1.1 Synthesis of $NdFeO_3$ nanoparticles (NFONP)

1.2 Synthesis of g-C_3N_4 nanoparticles

1.3 Photocatalytic CO_2 conversion activity measurements

1.4 Photocatalytic 2,4-DCP degradation activity measurements

1.5 Methanol-assisted H_2 evolution photocatalytic activity measurements

1.6 Photoluminescence (PL) spectroscopy measurements

1.7 Photoelectrochemical (PEC) Analysis

1.8 Hydroxyl free radical concentration measurements

1.9 Free radical trapping (Scavenger) experiments

1.10 FTIR spectroscopy measurements

1.11 BET surface area and pore diameter measurements

1.12 Computational Methodologies, DFT Calculations and Modeling Techniques

2. Supplementary Material Figures

3. Supplementary Material Tables (Table S1-S3)

4. Supplementary Material References

1. Experimental Section

1.1 Synthesis of $NdFeO_3$ nanoparticles (NFONP)

$NdFeO_3$ nanoparticles are prepared by the co-precipitation method. We dissolved $Nd(NO_3)_3$ and $Fe(NO_3)_3$ in DI H_2O to form 0.12 Molar solutions. After this, we stirred the solutions until the salts were completely dissolved. Accordingly, we slowly added 5% NaOH solution to the aforementioned solutions. Then, aged the mixture for 24 hours at room temperature. In the next step, we stirred the mixture occasionally to prevent settling and washed the precipitate with DI H_2O repeatedly to remove impurities. Accordingly, we centrifuged the mixture for 10 minutes at 5000 rpm to separate the solid from the liquid. In the next step, we dried the precipitate in an oven at 100 °C for 24 hours. After cooling, we ground the dried powder into a fine powder. Accordingly, the sample was put in a muffle furnace at 800 °C for 4 hours. The powder was

allowed to cool slowly to room temperature, and finally, the resultant sample was named $NdFeO_3$ nanoparticles. [1]

1.1 Synthesis of g-C_3N_4 nanoparticles

The nanosized g-C_3N_4 is prepared by employing our research group reported method.[2] In the standard experiment, we transferred 5 g of analytical-grade urea into a 100 mL ceramic crucible and heated it in a muffle furnace in air from room temperature to 550 °C at a heating rate of 10 °C min^{-1}, then hold the temperature at 550 °C for 4 h. The product was then allowed to cool naturally to room temperature. After this, the resulting product was ground into a fine powder and used throughout the experiments.

1.2 Photocatalytic CO_2 conversion activity measurements

The Photocatalytic CO_2 conversion activities are carried out by taking 0.21 g of nanocatalysts and uniformly dispersing them in 5.0 mL of DI H_2O. Accordingly, transferred into a cylindrical steel reactor with a volume of 100 mL with area of 3.51 cm^2. After this, pure CO_2 was run *via* a sintered-glass bubbler (20 μm pores), maintaining both moisture saturation (~3% v/v H_2O) and system pressure. After a 30-minute reaction equilibrium, the reaction system was subjected to a photocatalytic reaction. A continuous supply of CO_2 gas was maintained throughout the reaction under visible light sources (300 W Xe lamp, $\lambda \geqslant 400$ nm, 85 mW/cm^2). After each specific interval (1 h), 0.3 mL of the gaseous product was collected with a syringe and was subsequently injected into a gas chromatograph (Tech, GC-7920) which is supported by TCD and FID detectors along with N_2 carrier gas and a CO_2 converter. [3]

Notably, the apparent quantum efficiency (AQE) for CO_2 reduction was estimated using the total electron equivalents consumed for CO and CH_4 formation. The AQE was calculated using the following equation:

$$AQE(\%) = \frac{2n(CO) + 8n(CH_4)}{N_{photon}} \times 100$$

where $n(CO)$ and $n(CH_4)$ are the amounts of CO and CH_4 produced, respectively. The coefficients 2 and 8 represent the number of electrons required for CO_2 reduction to CO and CH_4, respectively. N_{photon} is the number of incident photons during irradiation.

1.3 Photocatalytic 2,4-DCP degradation activity measurements

The photocatalytic activities for 2,4-DCP degradation are conducted under visible light. In a typical experiment, 0.21 g of the photocatalyst was uniformly dispersed in 80 mL of 2,4-DCP solution (10.0 mg/L). Accordingly, transferred into a 250 mL Pyrex glass reactor. Prior to initiating the photocatalytic reaction, the resultant solution was stirred for 30 minutes in the absence of light to ensure equilibrium was attained. Subsequently, the reaction mixture was placed under a xenon lamp (300 W) and fitted with a visible-light cut-off filter (> 400 nm) for photocatalytic activity measurements. After a 1 h interval, a 5.0 mL sample of the solution was collected through a sterile syringe, and the collected product was checked by a UV-visible spectrophotometer (Shimadzu UV-2700) at a wavelength of 285 nm.[4]

1.4 Methanol-assisted H_2 evolution photocatalytic activity measurements

Methanol-assisted H_2 evolution photocatalytic activity was measured using a cylindrical quartz cell (250 mL volume, 7.50 cm^2 area). The assembly was connected to a sealed gas circulation system, and the generated products are analyzed trough TCD supported GC instrument (GC-9700), by utilizing nitrogen gas as the product carrier. In a typical photocatalytic activity measurement, 0.10 g of the sample powder was transferred into a solution mixture containing 85.0 mL of distilled H_2O and 25.0 mL of methanol. The resultant suspension was subsequently exposed to visible light using a xenon lamp (300 W) light source fitted with a visible-light cut-off filter (> 400 nm). The final gaseous product was tested by a GC instrument.[5]

1.5 Photoluminescence (PL) spectroscopy measurements

Photoluminescence spectra were recorded by a spectrofluorometer (PE LS 55) by operating it at (λ_{ex} = 325 nm, λ_{em} = 460 nm). The spectrophotometer was operated in excitation and emission modes.[6]

1.6 Photoelectrochemical (PEC) Analysis

In the standard method, 0.10 g of nanoctalysts, 1mL of IPA, 0.10 g of PEG, 0.05 mL of PEG, and 0.05 mL of acetylacetone are placed into a small vial and allowed to sonicate, followed by stirring for 3 h in order to obtain a uniform solution. Subsequently, followed by more 3 days of stirring to achieve a consistent paste. The resulting colloidal pastes were applied uniformly on FTO glass substrates. Accordingly, the FTO-glass piece (2.0 cm × 4.0 cm) was thermally treated in a muffle furnace at 450°C for a duration of 0.5 hours. In all photoelectrochemical

(PEC) analysis, a 3-electrode system was employed, utilizing the photocatalyst as a working electrode, a KCl-saturated Ag/AgCl electrode as a reference electrode, and Pt plate as a counter electrode. Adding more, A 0.50 M sodium sulphate solution was employed as an electrolyte. Notably, all experiments were conducted in a quartz cell under a xenon lamp (300 W) with a 420 nm filter, providing visible-light irradiation ($\lambda \geq 400$ nm). An electrochemical workstation V13806 (model IVIUM, China) was used for all PEC analysis. [7]

1.7 Hydroxyl free radical concentration measurements

The •OH radicals generated during various types of photo (electro) chemical reactions are identified by fluorescence spectroscopy (FS). In the standard experiment, the photocatalyst (50 mg) was dispersed in coumarin solution (0.05 g/L to make a 50 mL solution). After this, the solution was transferred into a reaction vessel and subjected to irradiation for 60 min under visible light using a xenon lamp (300 W) light source fitted with a visible-light cut-off filter (> 400 nm), with vigorous stirring throughout the process. Accordingly, 2 mL samples were collected and tested.[8]

1.8 Free radical trapping (Scavenger) experiments

Free radical trapping (Scavenger) experiments were conducted to validate the photocatalytic mechanism and determine the reactive species participating in the organic pollutant degradation process. In a typical experiment, three distinct scavengers were systematically employed to identify reactive species, i.e EDTA-2Na for trapping photogenerated holes, isopropanol for quenching hydroxyl radicals (•OH), and p-benzoquinone for trapping superoxide radicals ($\bullet O_2^-$). Notably, each scavenger was introduced separately to trap its respective reactive species. In the standard experimental procedure, EDTA-2Na, IPA, and BQ were added separately to the 2,4-DCP-containing solution and allowed to stir for 1 h under a Xe lamp. Subsequently, 5.0 mL of the solution was collected, filtered, and tested by UV (285 nm). [9]

1.9 FTIR spectroscopy measurements

FTIR spectra of the samples were obtained using an FTIR spectrometer (BRUKER, Germany). KBr served as the diluent in all FT-IR analysis. [10]

1.10 BET surface area and pore diameter measurements

The BET surface area of the samples was tested by utilizing a Micromeritics Tristar II 3020 analyzer and employing nitrogen adsorption-desorption at -196 °C. Initially, the samples were preheated at 150 °C to remove moisture. [11]

1.11 Computational Methodologies, DFT Calculations and Modeling Techniques

Computational methodologies, DFT calculations and modeling techniques were performed to investigate the electronic structure, interfacial charge transfer, different pathways, and CO_2 reduction mechanism of our prepared samples. All calculations were carried out using the Quantum ESPRESSO package based on the plane-wave pseudopotential method. The Perdew–Burke–Ernzerhof (PBE) functional within the generalized gradient approximation (GGA) was applied for exchange-correlation interactions. The kinetic energy cutoff and charge density cutoff were set to 50 Ry and 425 Ry, respectively. A Monkhorst–Pack k-point mesh of 6 × 6 × 8 was used for DOS and PDOS calculations.

The adsorption energies of CO_2 reduction intermediates were calculated using Equation (1):

$$\Delta E_{ads.} = (E_{Adduct}) - (E_{catalyst} + E_{Intermediate}) \qquad (1)$$

$$\Delta G = \Delta E + \Delta ZPE - T\Delta S - neU + kTln10 \times \Delta pH \qquad (2)$$

Where, $E_{catalyst-Intermediate}$, $E_{catalyst}$, and $E_{Intermediate}$ are the energies of the intermediate-adduct, catalyst, and Intermediate, respectively. ΔG, ΔZPE, and $T\Delta S$, and ΔE represent the reaction energies, zero-point energy, and entropy variation, whereas n, U, and T are the electron transfer number, electrode potential, and temperature, respectively [12]. The charge density difference was calculated using Equation (3).

$$\Delta\rho_{(\text{Density Difference})} = \rho_{(Adduct)} - \rho_{(catalyst)} - \rho_{(intermediate)} \quad (3)$$

2. Supplementary Material Figures (Figure S1- Figure S9)

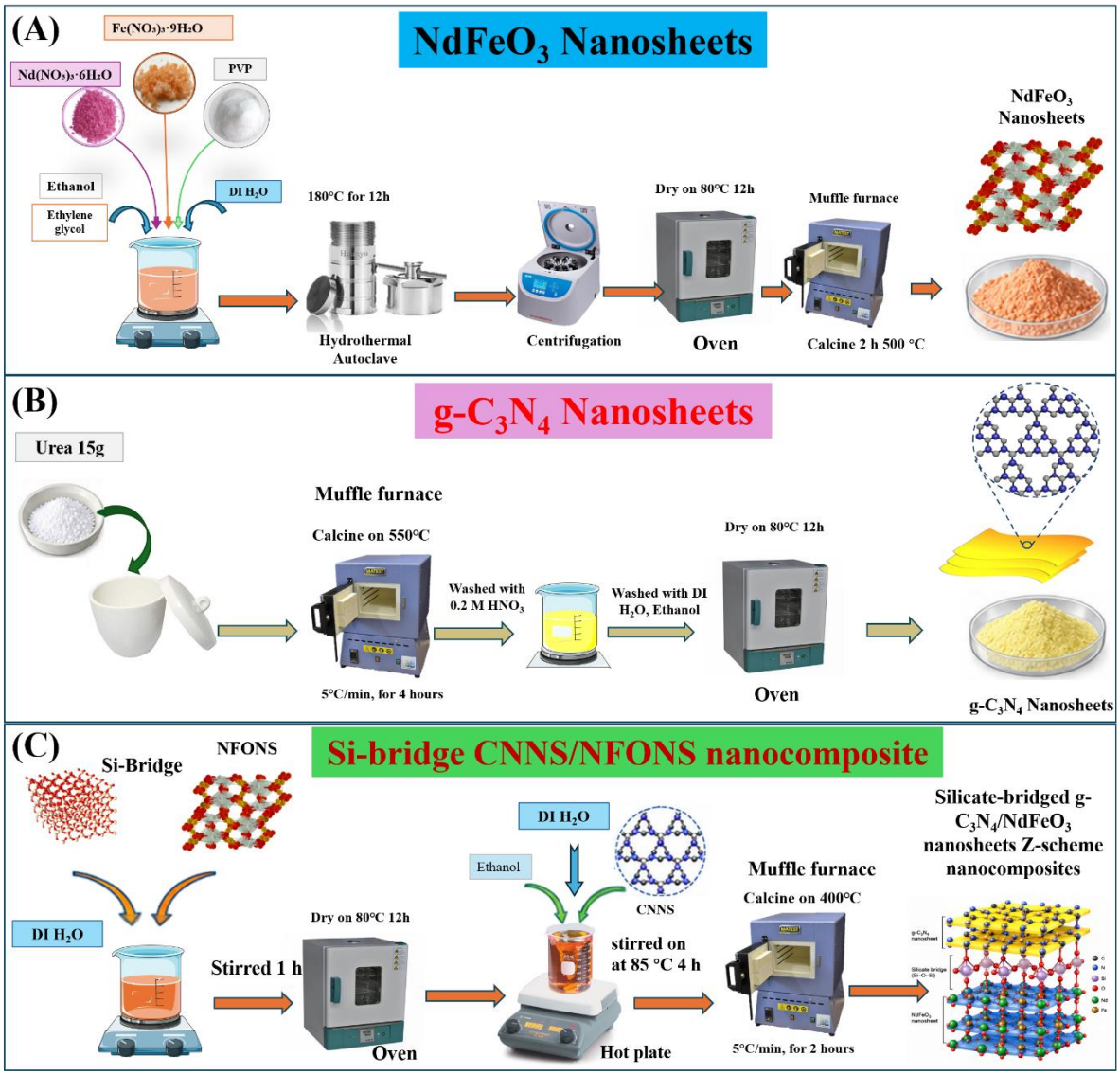


Figure S1. Comprehensive synthesis scheme for $NdFeO_3$ nanosheets (A), g-C_3N_4 nanosheets (B), and Silicate-bridged g-C_3N_4/$NdFeO_3$ nanosheets Z-scheme nanocomposites (C).

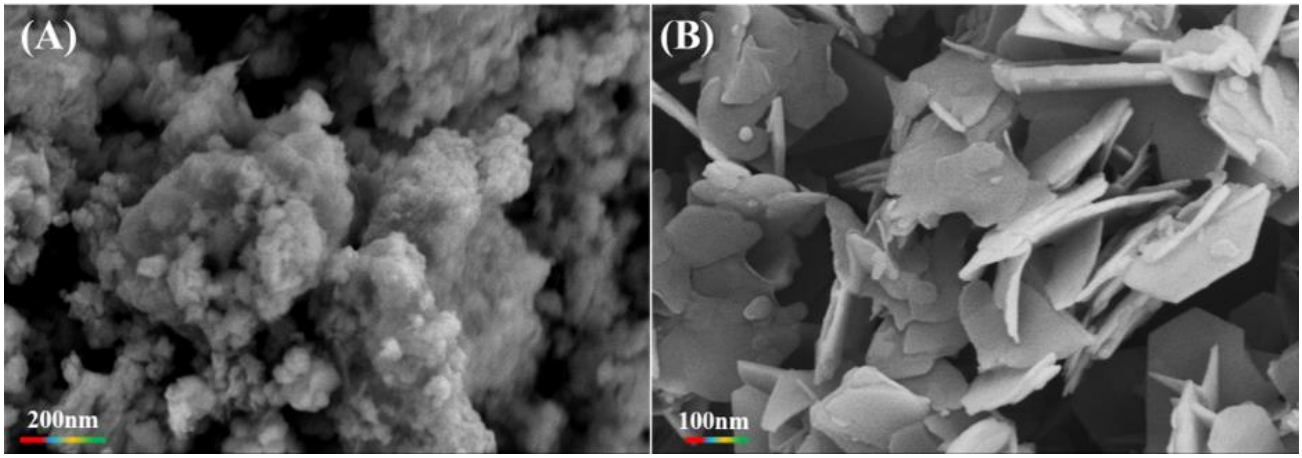


Figure S2. SEM images of NFONP (A) and NFONS (B).

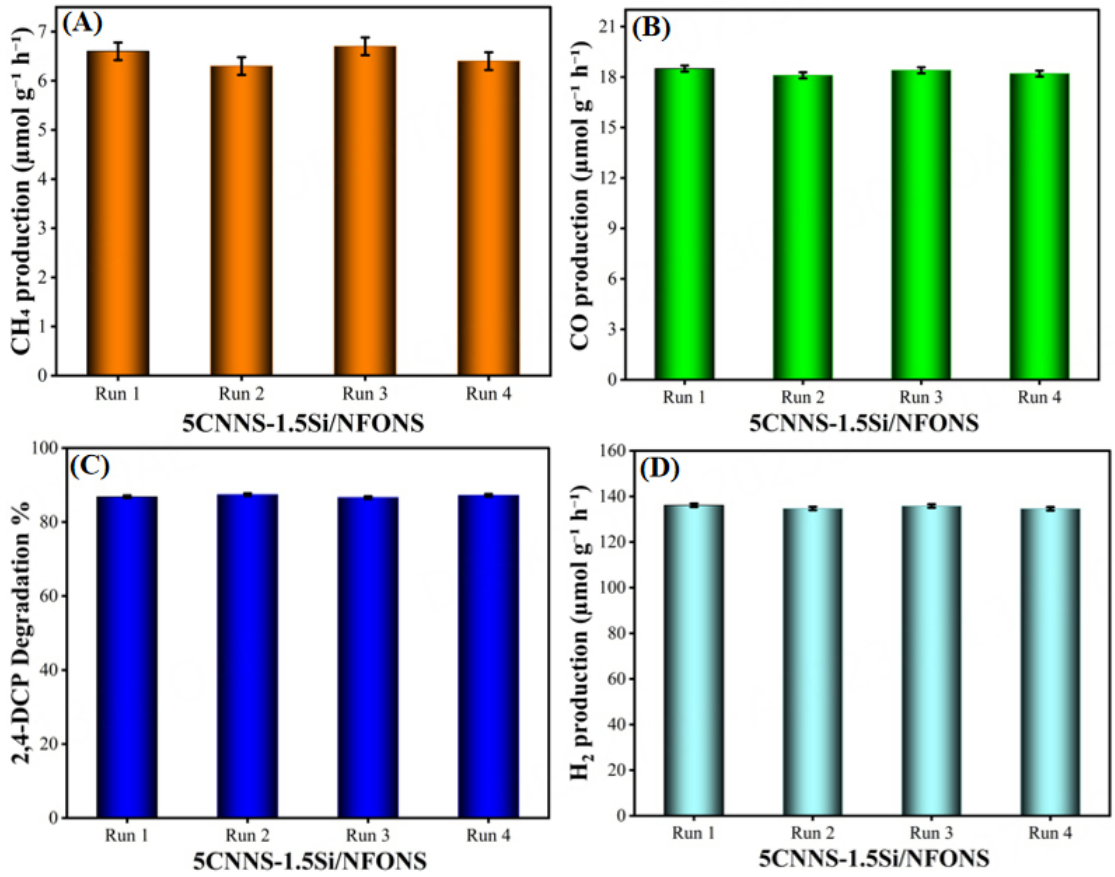


Figure S3. Reusability and performance stability of 5CNNS-1.5Si/NFONS over four consecutive reaction cycles using the same catalyst sample: (A) CH_4 production rate, (B) CO production rate, (C) 2,4-DCP degradation efficiency, and (D) H_2 production rate. Error bars represent the standard deviation (SD) calculated across the four consecutive reaction cycles (n = 4).

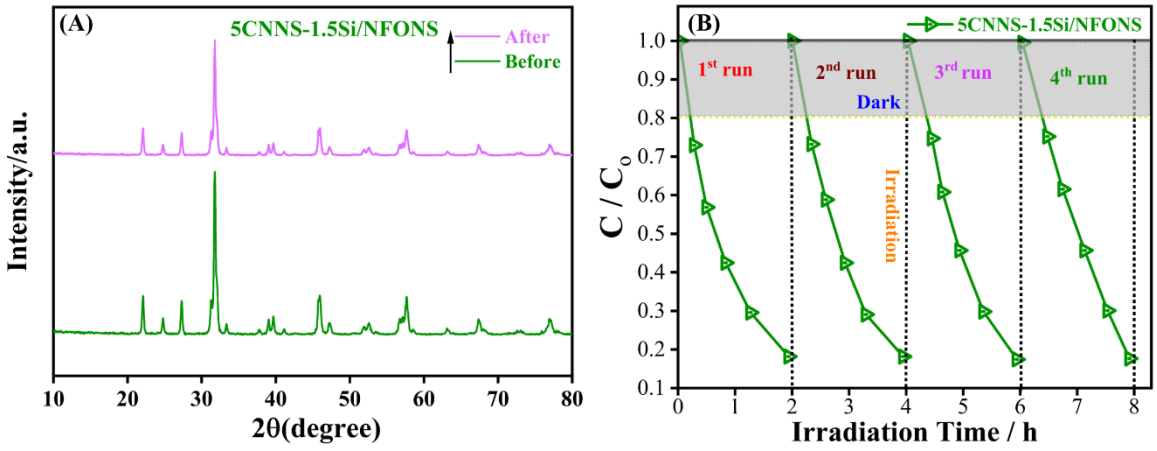


Figure S4. XRD patterns (A), photocatalytic activities, recyclability, and reusability test of 2,4-DCP degradation (B) of the 5CNNS-1.5Si/NFONS nanocomposite before and after utilization.

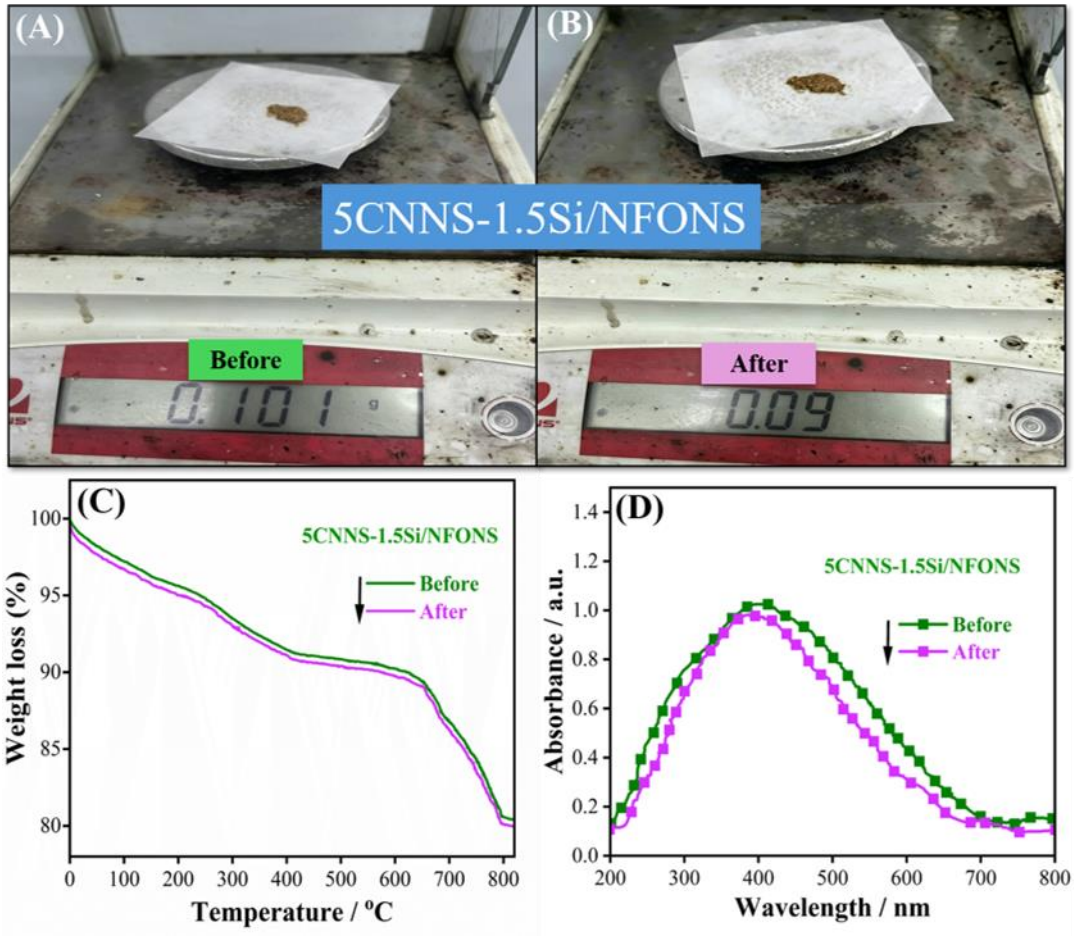


Figure S5. Weight stability tests (A, B), TGA Curves (C), and UV-Visible absorbance spectra (D) of 5CNNS-1.5Si/NFONS nanocomposite before and after utilization.

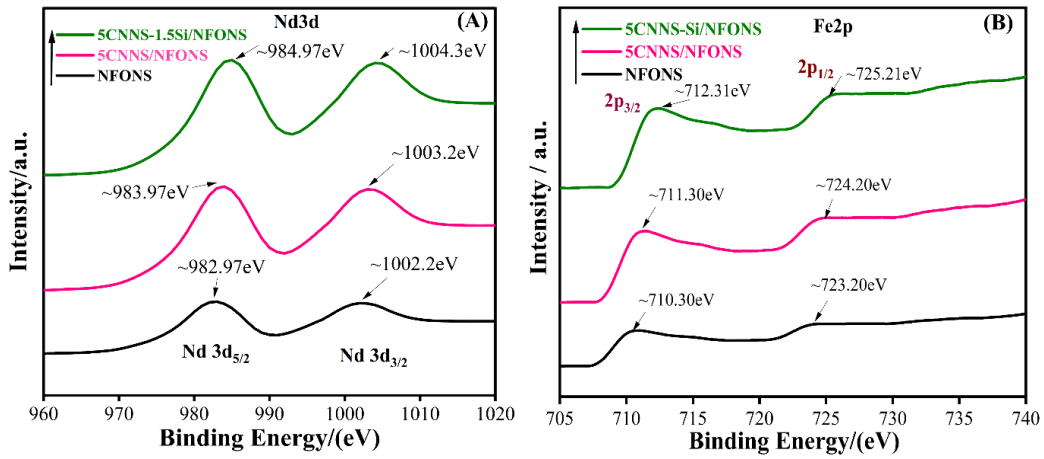


Figure S6. High-resolution XPS spectra of Nd3d (A) and Fe2P (B), of NFONS, 5CNNS/NFONS, and 5CNNS-1.5Si/NFONS.

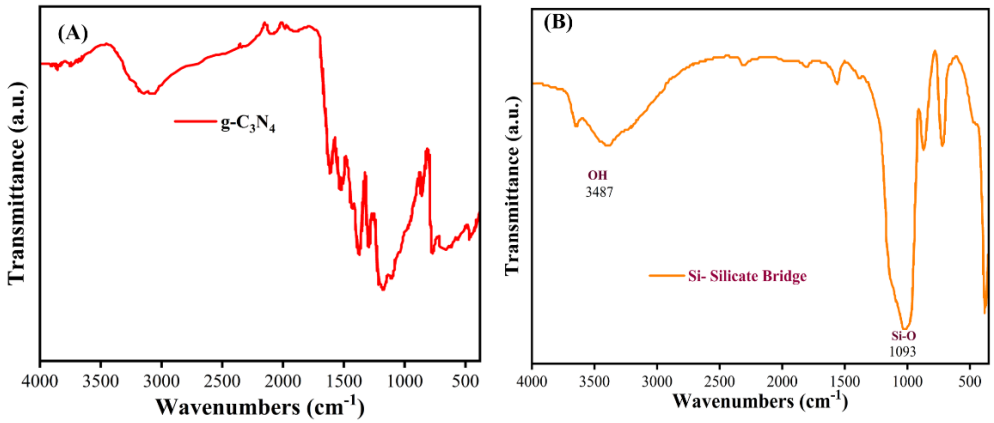


Figure S7. FTIR spectra of g-C_3N_4 (A) and Si-O bridge (B).

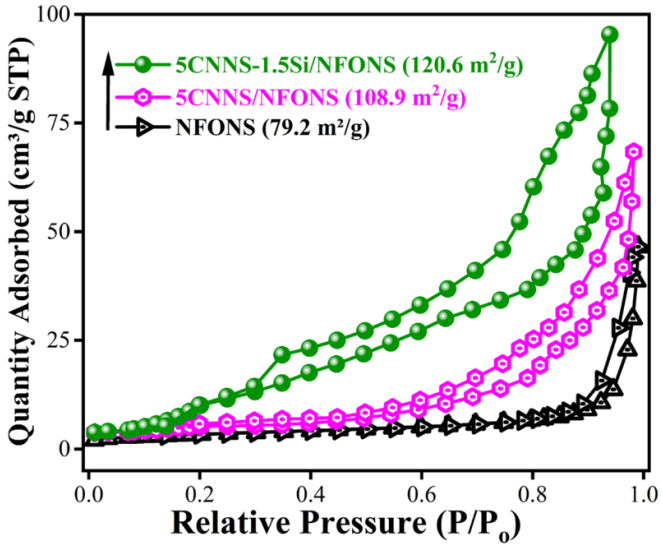


Figure S8. BET surface areas of NFONS, 5CNNS/NFONS, and 5CNNS-1.5Si/NFONS.

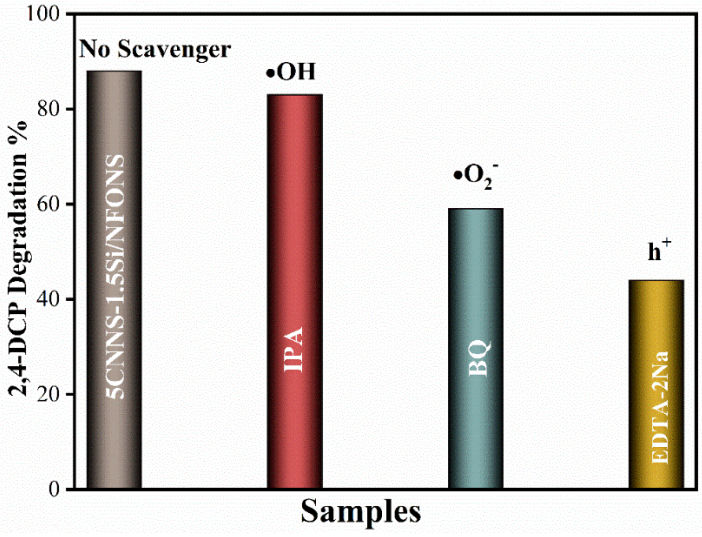


Figure S9. Free radical trapping experiment of 5CNNS-1.5Si/NFONS.

3. Supplementary Material Tables (Table S1-Table S3)

Table S1. List of abbreviations and acronyms used in this manuscript.

Abbreviations	Definition	Abbreviations	Definition
NFO	$NdFeO_3$	**Si–O**	Silicate–Oxide
NFONP	$NdFeO_3$ Nanoparticles	**PL**	Photoluminescence
NFONS	$NdFeO_3$ Nanosheets	**FS**	Fluorescence spectroscopy
CNNP	g-C_3N_4 Nanoparticles	**PEC**	Photo electrochemical
CNNS	g-C_3N_4 Nanosheets	**TPD**	Temperature-Programmed Desorption
g-C_3N_4	Graphitic Carbon Nitride	**EC**	Electrochemical
2,4-DCP	2,4-Dichlorophenol	**PDS**	Potential-determining step
BQ	Benzoquinone	**QE**	Quantum Efficiency
PVP	Polyvinylpyrrolidone	**Ov**	Oxygen Vacancy
IPA	Isopropyl Alcohol	**h^+**	Holes
EDTA-2Na	Ethylenediaminetetraacetic Acid Disodium Salt	**•OH**	Hydroxyl Radicals
VB	Valence Band	**$•O_2^-$**	Superoxide Radicals
CB	Conduction Band	**CO_2-TPD**	CO_2 Temperature-Programmed Desorption
BET	Brunauer–Emmett–Teller Method for Surface Area Measurement	**FTIR**	Fourier-Transform Infrared Spectroscopy
TGA	Thermogravimetric Analysis	**FTO**	Fluorine-Doped Tin Oxide
XPS	X-Ray Photoelectron Spectroscopy	**HRTEM**	High-Resolution Transmission Electron Microscopy
UV–Vis DRS	Ultraviolet–Visible Diffuse Reflectance Spectroscopy	**SEM**	Scanning Electron Microscopy

TEM	Transmission Electron Microscopy	**KPFM**	Kelvin Probe Force Microscopy
EIS	Electrochemical Impedance Spectroscopy	**GC**	Gas Chromatography
JCPDS	Joint Committee on Powder Diffraction Standards	**FID**	Flame Ionization Detector
TCD	Thermal Conductivity Detector	**AQE**	Apparent Quantum Efficiency

Table S2. Statistical and reusability analysis of CO_2-to-CH_4, CO_2-to-CO, and H_2 evolution rates performed in independent runs (n = 4). Values are presented as mean ± standard deviation.

Experiment	Sample	Run 1	Run 2	Run 3	Run 4	Average ± SD
$CO_2 \rightarrow CH_4$ (µmol g^{-1} h^{-1})	NFONS	0.43	0.46	0.44	0.47	0.45 ± 0.02
	5CNNS/NFONS	3.00	3.15	3.10	3.15	3.10 ± 0.07
	5CNNS-1Si/NFONS	3.80	3.95	3.90	3.95	3.90 ± 0.07
	5CNNS-1.5Si/NFONS	6.60	6.30	6.70	6.40	6.50 ± 0.18
	5CNNS-2Si/NFONS	4.70	4.90	4.80	4.80	4.80 ± 0.08
	5CNNS-2.5Si/NFONS	5.20	5.40	5.30	5.30	5.30 ± 0.08
$CO_2 \rightarrow CO$ (µmol g^{-1} h^{-1})	NFONS	1.25	1.32	1.28	1.35	1.30 ± 0.04
	5CNNS/NFONS	8.61	8.73	8.87	8.99	8.80 ± 0.17
	5CNNS-1Si/NFONS	10.20	10.50	10.40	10.50	10.40 ± 0.14
	5CNNS-1.5Si/NFONS	18.50	18.10	18.40	18.20	18.30 ± 0.18
	5CNNS-2Si/NFONS	11.40	11.80	11.60	11.60	11.60 ± 0.16

	5CNNS-2.5Si/NFONS	13.00	13.40	13.20	13.20	13.20 ± 0.16
2,4-DCP degradation (%)	NFONS	11.8	12.2	11.9	12.1	12.0 ± 0.18
	5CNNS/NFONS	58.5	59.4	58.8	60.3	59.3 ± 0.79
	5CNNS-1Si/NFONS	64.5	65.4	64.8	66.3	65.3 ± 0.79
	5CNNS-1.5Si/NFONS	86.8	87.4	86.6	87.2	87.0 ± 0.37
	5CNNS-2Si/NFONS	69.5	70.4	69.8	70.3	70.0 ± 0.42
	5CNNS-2.5Si/NFONS	74.5	75.4	74.8	75.3	75.0 ± 0.42
H_2 evolution ($\mu mol\ g^{-1}\ h^{-1}$)	NFONS	50.6	51.5	51.0	51.7	51.2 ± 0.50
	5CNNS/NFONS	95.2	96.8	96.0	97.6	96.4 ± 1.03
	5CNNS-1Si/NFONS	107.5	109.3	108.4	109.6	108.7 ± 0.95
	5CNNS-1.5Si/NFONS	136.1	134.7	135.8	134.6	135.3 ± 0.76
	5CNNS-2Si/NFONS	111.6	113.4	112.5	113.7	112.8 ± 0.95
	5CNNS-2.5Si/NFONS	114.9	116.8	115.7	117.0	116.1 ± 0.98

Table S3. The photocatalytic process initiated under visible light over the Si-Bridge-mediated g-C_3N_4/$NdFeO_3$ Z-scheme heterojunction for CO_2 conversion, 2,4-DCP degradation, and H_2 generation mechanism

Steps#	**Photocatalytic Process**	**Equation**
1	CNNS+hν→CNNS$\left(e_{CB}^{-}+h_{VB}^{+}\right)$	……...**i**
2	NFONS+hν→NFONS$\left(e_{CB}^{-}+h_{VB}^{+}\right)$	……...**ii**
3	NFONS(e_{CB}^{-})+CNNS$\left(h_{VB}^{+}\right)$→Recombination *via* Si-O bridge	……...**iii**
4	$2H_2O + 4h^+$ (NFONS) → $O_2 + 4H^+$	……...**iv**
5	CNNS$(e_{CB}^{-})+O_2\rightarrow\cdot O_2^{-}$	……...**v**

6	$2H^+ + 2e^- \rightarrow H_2$	……...**vi**
7	$CO_2 + 2H^+ + 2e^- \rightarrow CO + H_2O$	……..**vii**
8	$CO_2 + 8H^+ + 8e^- \rightarrow CH_4 + 2H_2O$	……**viii**
9	2,4-DCP+h^+_{VB}(NFONS)→Oxidized Intermediates	……...**ix**
10	2,4-DCP/Intermediates+$\cdot O_2^-$→ Further Oxidized Intermediates	……...**x**
11	Intermediates+$h^+ / \cdot O_2^- \rightarrow CO_2 + H_2O + Cl^-$	……...**xi**

4. Supplementary Material References

1 Sarang, P. R. & Lad, V. N. Synthesis, characterization and Langmuir-Blodgett film deposition of NdFeO3 nanoparticles. *Physica B: Condensed Matter* **738**, 418827, doi:https://doi.org/10.1016/j.physb.2026.418827 (2026).

2 Saeed, M., Asghar, H., Khan, I., Akram, N. & Usman, M. Synthesis of TiO2-g-C3N4 for efficient photocatalytic degradation of Congo Red dye. *Catalysis Today* **447**, 115154, doi:https://doi.org/10.1016/j.cattod.2024.115154 (2025).

3 Fang, S. *et al.* Photocatalytic CO2 reduction. *Nature Reviews Methods Primers* **3**, 61, doi:10.1038/s43586-023-00243-w (2023).

4 Mohamadpour, F. & Amani, A. M. Photocatalytic systems: reactions, mechanism, and applications. *RSC Advances* **14**, 20609-20645, doi:10.1039/d4ra03259d (2024).

5 Lu, L. *et al.* Spinodal decomposition enables coherent plasmonic metal/semiconductor heterostructure for full spectrum photocatalysis. *Nature Communications* **16**, 6479, doi:10.1038/s41467-025-61872-1 (2025).

6 Mitchell, E., Law, A. & Godin, R. Experimental determination of charge carrier dynamics in carbon nitride heterojunctions. *Chemical Communications* **57**, 1550-1567, doi:10.1039/d0cc06841a (2021).

7 Rabell, G. O., Alfaro Cruz, M. R. & Juárez-Ramírez, I. Photoelectrochemical (PEC) analysis of ZnO/Al photoelectrodes and its photocatalytic activity for hydrogen production. *International Journal of Hydrogen Energy* **47**, 7770-7782, doi:https://doi.org/10.1016/j.ijhydene.2021.12.107 (2022).

8 Nosaka, Y. & Nosaka, A. Y. Generation and Detection of Reactive Oxygen Species in Photocatalysis. *Chemical Reviews* **117**, 11302-11336, doi:10.1021/acs.chemrev.7b00161 (2017).

9 Wang, G. *et al.* Hydroxyl, hydroperoxyl free radicals determination methods in atmosphere and troposphere. *Journal of Environmental Sciences* **99**, 324-335, doi:https://doi.org/10.1016/j.jes.2020.06.038 (2021).

10 Thomas, A. *et al.* Graphitic carbon nitride materials: variation of structure and morphology and their use as metal-free catalysts. *Journal of Materials Chemistry* **18**, 4893-4908, doi:10.1039/b800274f (2008).

11 Osterrieth, J. W. M. *et al.* How Reproducible are Surface Areas Calculated from the BET Equation? *Advanced Materials* **34**, 2201502, doi:https://doi.org/10.1002/adma.202201502 (2022).

12 Gholami, D. *et al.* In situ growth of CuFeS2/CuS bridged heterojunction catalyst with mixed redox-couple cations for excellent photocatalytic degradation of organophosphate insecticide: CFD and DFT modeling. *Chemical Engineering Journal* **461**, 141950, doi:https://doi.org/10.1016/j.cej.2023.141950 (2023).